Section 8

Development of and advances in ocean modelling and data assimilation, sea-ice modelling, wave modelling

Modeling the M_2 and O_1 Baroclinic Tides in the Gulf of Mexico using the HYbrid Coordinate Ocean Model (HYCOM)

Flavien Gouillon, Benoit Vannière, Alexandra Bozec and Eric Chassignet
Center for Ocean-Atmospheric Prediction Studies
The Florida State University
gouillon@coaps.fsu.edu

This study focuses on modeling the baroclinic tidal dynamic in the Gulf of Mexico. In particular, the study addresses the importance of tidal energy conversion in the interior of this basin. A recent paper by *Gouillon et al.* (in review, 2009) computed new estimates of tidal energetics in the Gulf of Mexico using a high resolution model of a barotropic ocean, thus assuming that the bottom friction was the only mechanism for tidal dissipation. Here, we investigate the importance of the tidal conversion process as a contributor to the dissipation of the barotropic tide by considering a baroclinic ocean.

Numerical experiments are conducted with the HYbrid Coordinate Ocean Model (HYCOM) (*Bleck*, 2002) with high horizontal resolution (1/25°). HYCOM is run in a fully isopycnal mode. There is no bottom friction to isolate the tidal conversion process and no diapycnal mixing is prescribed. The initial stratification is the monthly mean of August (summer) when the stratification is the strongest in the GOM. The tides are the only forcing present in the model runs. The tidal forcing is implemented by setting elevations and depth-independent velocities along the open boundaries of the model (Caribbean Sea and Florida Keys) obtained by the North Atlantic 2D model of *Egbert et al.* (*Egbert and Erofeeva*, 2002). Here we considered 2 tidal constituents: M_2 and O_1 tide (12.421 hr and 25.81 hr, tidal period respectively). In the GOM, the K_1 tide is similar to the O_1 tide and the S_2 tidal constituent signal is negligible.

Figure 1 shows the tidal amplitudes and tidal phases in the domain for a) the M_2 tide and b) the O_1 tide. A qualitative evaluation of these results shows that they are in good agreement with previous studies such as *Reid and Whitaker* (1981), and more recently *He and Weisberg* (2002) and *Kantha* (2005). A qualitative validation of the simulated baroclinic tides is made by comparing the results against 62 tidal gauges located around the Gulf of Mexico. The Figure 2 shows: a) the histogram of the difference between observed and modeled tidal amplitudes and b) the histogram of the directional distance. It is clear that both tidal amplitude and phase are well represented in HYCOM.

Estimates of the tidal baroclinic energy are computed in the basin. The depth integrated baroclinic energy densities are computed following *Martini et al.* (2007):

$E = \frac{\rho_0}{2}\int_{-H}^{0}\left\langle u^2 + v^2 \right\rangle_t dz + \frac{\rho_0}{2}\int_{-H}^{0}\left\langle N^2 \zeta^2 \right\rangle_t dz$, where, u and v are the eastward and the northward velocities, respectively, ζ the vertical displacement, N the buoyancy frequency spatially averaged over the domain, ρ_0 the average density and H the bottom depth. Figure 3a shows that most of the baroclinic energy is in the vicinity of the West Florida Shelf (WFS) and that most of this energy is trapped in the eastern basin. As the internal waves propagate away from their generation site (WFS), they quickly dissipate as the cross vertical section in Figure 3b shows.

Since the Gulf of Mexico is considered a flat basin, we expect negligible baroclinic tidal energy in the GOM. This is confirmed by the above findings although strong baroclinic tidal energy exists near the Yucatan Shelf and the WFS.

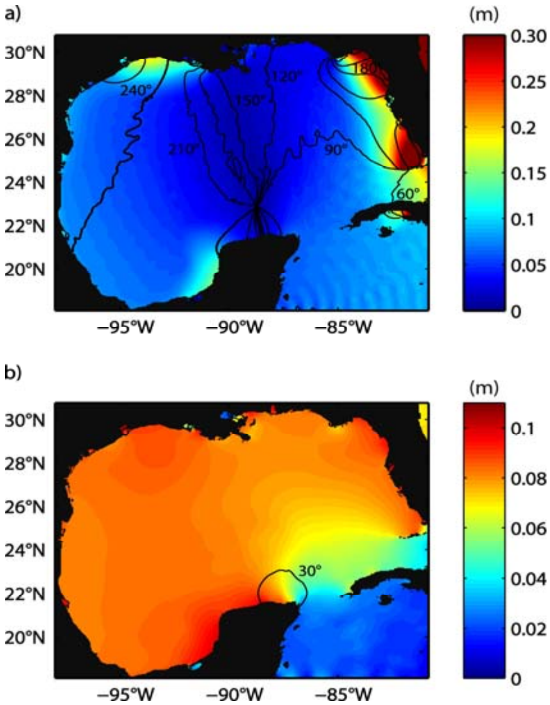

Figure 1: Tidal amplitudes and phases for a) M2 and b) O1

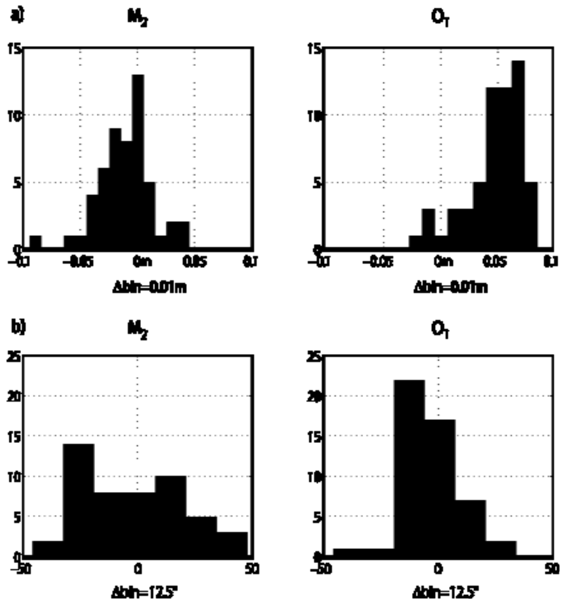

Figure2: M2 and O1 histograms of a) difference between observation and model and b) directional distance

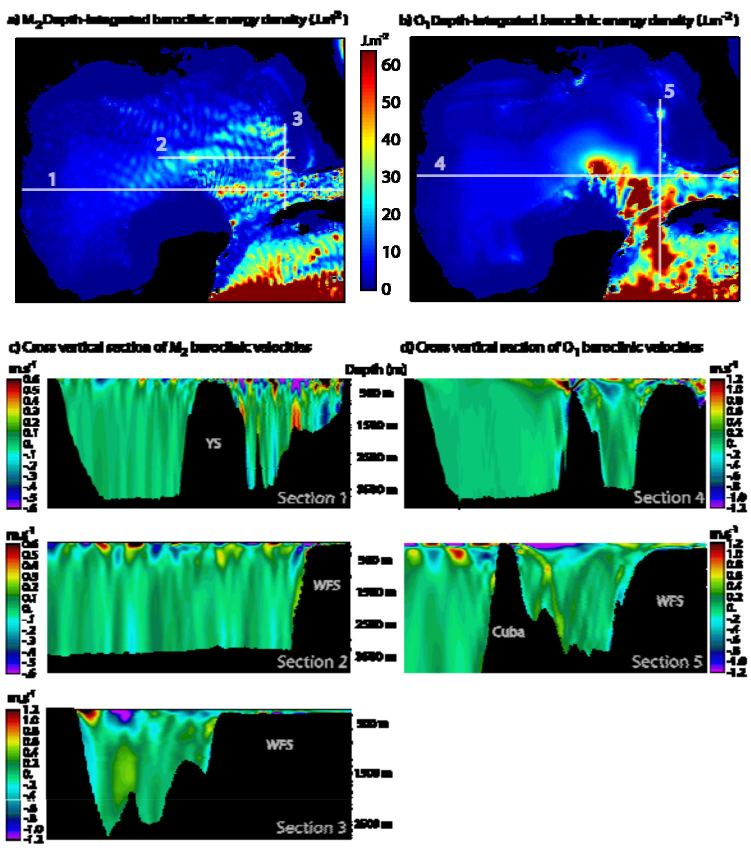

Figure 3

Circulation and transport on the Northeastern Gulf of Mexico Shelf using a high-resolution ROMS model

Austin C. Todd and Steven L. Morey
Center for Ocean-Atmospheric Prediction Studies, Florida State University, Tallahassee, Florida, USA
todd@coaps.fsu.edu

Introduction

Several studies over the past decade have demonstrated the immense variability of the West Florida Shelf (WFS) and Gulf of Mexico (GOM) shelf circulations on various time scales (e.g. He and Weisberg 2002, Morey et al. 2005, Weisberg et al. 2005). However, further questions remain about the ramifications of the shelf circulation on the cross-shelf transport. A relevant example is the onshore transport of pelagic gag grouper (*Mycteroperca microlepis*) larvae from spawning grounds along the WFS break (~70m depth) in February – April to inshore sea grass beds (<5m depth) some 45-60 days later. Previous collaborative works between biologists and physical oceanographers (e.g. Fitzhugh et al. 2005) have resolved little about the mechanisms responsible for onshore transport of these larvae in the spring. Furthermore, Fitzhugh et al. (2005) have voiced the need for three-dimensional modeling approaches in order to better understand the complexity of this problem. We assess the circulation and subsequent transport in the Big Bend Region (BBR) of the WFS using a high-resolution modeling approach (Figure 1).

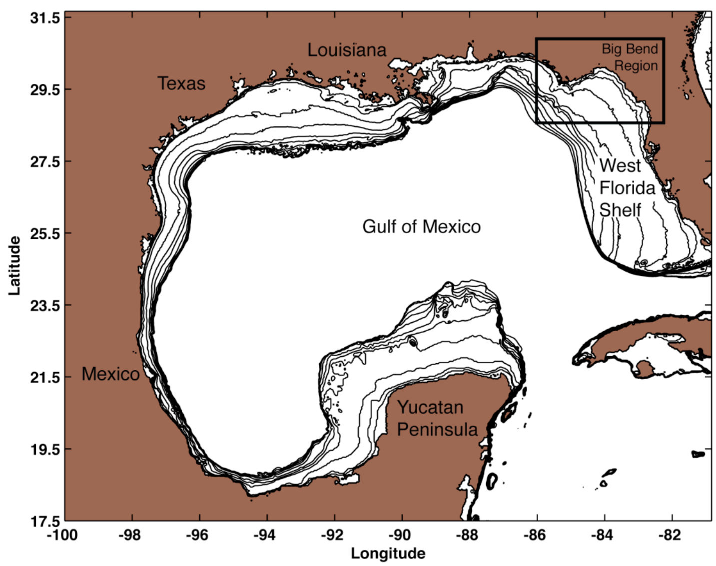

Figure 1. Gulf of Mexico with ROMS model domain indicated by the black box in the northeast corner.

Objectives and Methods

This study is focused on simulating the shelf circulation in the BBR for several different years, although only results for 2007 are provided herein. We use a 30 arcsec (800-900m) resolution Regional Ocean Modeling System (ROMS) configuration with 25 vertical layers, North American Regional Reanalysis (NARR) 3-hourly winds, 16 river sources, COARE 3.0 bulk flux algorithm, and open boundary conditions forced by the Global HyCOM model. Only the spring (01 Feb – 30 Jun) circulation is assessed, as this is the time during which gag spawn and their larvae are subsequently transported inshore.

The location of gag larvae in the water column is unknown, and surface currents at this time of the year are typically offshore. Thus, various water depths are tested in this model to determine the layer in which particles will most successfully arrive inshore. Furthermore, basic Ekman layer theory and upwelling circulation theory suggests onshore transport should occur in the bottom layer during this time of the year (with mean winds from the North – Northwest). To test this theory, trajectories are calculated for particles released in bottom, surface, and mid-depth layers at various spots along the northeastern GOM shelf break.

Results

Results for 2007 indicate an overwhelming number of particles in the bottom layer arrive inshore, associated with a large upwelling event (Figure 2). Furthermore, few particles advected in the surface layer or at mid-depth reach the inshore sea grass beds in the BBR (< 5m) (Figure 3). In the surface layer and at mid-depths, only 0.04% of all particles released are advected shallower than 5m in the BBR, however 7.67% of all particles released in the bottom layer are advected shallower than 5m in the BBR. A maximum success rate of over 99% of particles released in a single day occurs in early April for the bottom layer (Figure 3). This evidence supports the idea of larval transport in the bottom layer, and emphasizes the usefulness of three-dimensional models toward this interdisciplinary study.

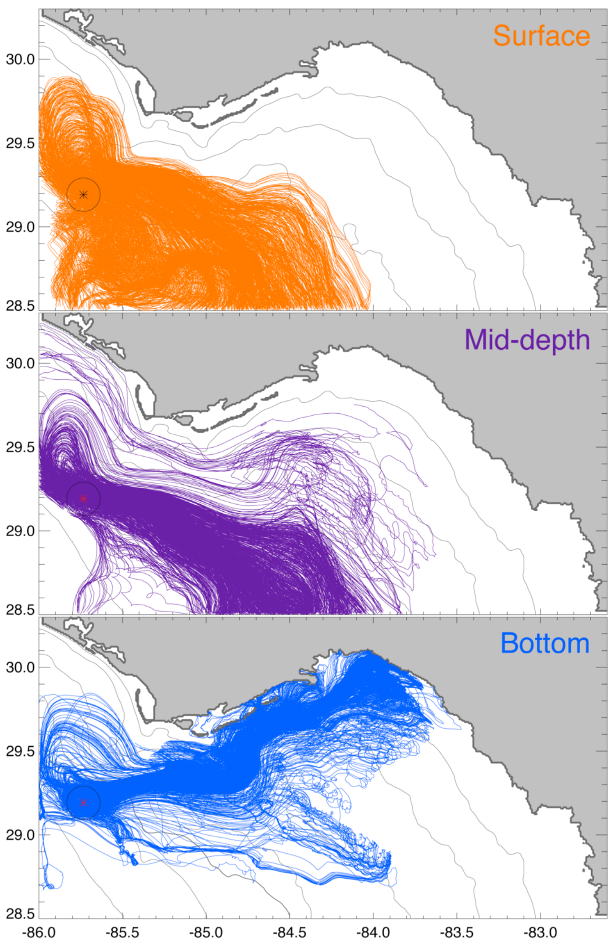

Figure 2. Particle trajectories in layers 1, 13, and 25, for bottom, mid-depth, and surface layers, respectively. 25 particles are seeded every 3 hours for one week beginning on 31 March 2007 about a 0.1-degree radius of a single seeding location. Each particle is followed for 45 days.

References

Fitzhugh, G.R., C .C. Koenig, F.C. Coleman, C.B. Grimes, and W. Sturges, 2005: Spatial and temporal patterns in fertilization and settlement of young gag (Mycteroperca Microlepis) along the West Florida Shelf, Bul l. of Marine Science, 77(3), 377-396.

He, R. and R.H. Weisberg, 2002: West Florida shelf circulation and temperature budget for the 1999 spring transition, Cont. Shelf Res., 22, 719-748

Morey, S., J. Zavala-Hidalgo, and J.J. O'Brien, 2005: The seasonal variability of continental shelf circulation in the northern and western Gulf of Mexico from a high-resolution numerical model, Circulation in the Gulf of Mexico: Observations and Models, AGU Geophysical Monograph Series 161, 203-218

Weisberg, R.H., R. He, Y. Liu, J.I. Virmani, 2005: West Florida shelf circulation on synoptic seasonal, and interannual time scales, Circulation in the Gulf of Mexico: Observations and Models, AGU Geophysical Monograph 161, 325-346

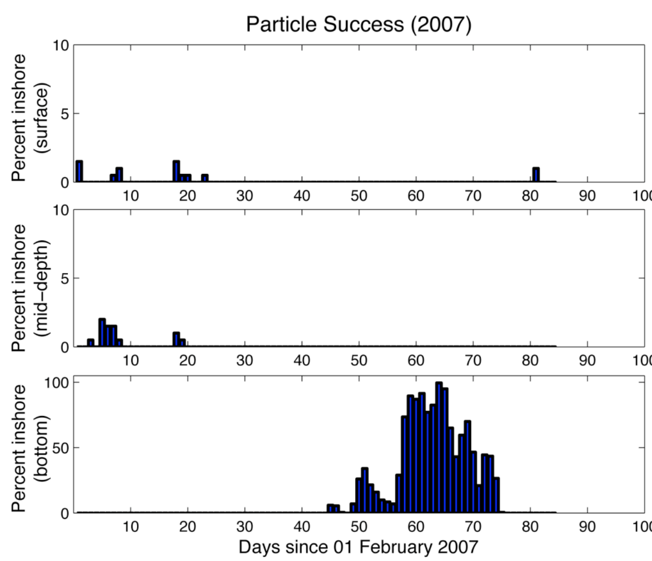

Figure 3. Success rate of particles reaching water shallower than 5m to the east of Cape San Blas within 45 days of being seeded. Days represent the day on which particles were seeded. Note the percentage different scales.

Numerical simulation for the ocean response to Typhoons Tina and Winnie in 1997 and their relations to sudden variations of pCO$_2$.

Akiyoshi Wada [1*] and Takashi Midoriwaka [1]

1) Meteorological Research Institute, Tsukuba, Ibaraki, 305-0052, JAPAN

*awada@mri-jma.go.jp

1. Introduction

An automatic-measuring system for the partial pressure (pCO$_2$) of atmospheric and oceanic carbon dioxide mounted on the moored buoy in the East China Sea (28°10'N, 126°20'E) captured sudden variations of oceanic pCO2 during the passage of Typhoons Tina and Winnie in 1997 (Nemoto et al., 2009). In order to investigate dynamics and thermodynamic associated with the sudden variations of oceanic pCO$_2$, we perform numerical simulations associated with the oceanic response to Tina and Winnie using the Meteorological Research Institute Community Ocean Model (Ishikawa et al., 2005).

2. Experiment Design

First, we perform a numerical simulation using the North Pacific version of MRI.COM. The integration time is 2 months with nudging daily data of sea temperature and salinity on 3 August 1997, obtained from the oceanic reanalysis data. Second, we perform a numerical simulation by the same version of MRI.COM except that the integration time is 21 days and the run is performed without nudging daily data of sea temperature and salinity on 3 August 1997. The purpose of the second run is to make initial and lateral boundary conditions for the third run. Third, we perform a numerical simulation using the regional version of MRI.COM. The integration time is 21 days, which is the same as the second run. However, the computational domain for the regional model is 10-50°N, 120-160°E. The horizontal resolution is 0.25° and the number of vertical levels is 54. The time step is 10 minutes. The mixed-layer scheme of Noh and Kim (1999) is used now. These three procedures are the same as those of Wada et al., (2009).

NCEP R2 atmospheric reanalysis dataset with a grid spacing of 1.875° is used for making atmospheric forcings such as short-wave and long-wave radiation, sensible and latent heat fluxes, water flux and wind stress. In addition, the Rankine vortex created by using the RSMC best-track data is used for the third run (see Wada et al., 2009). Short-eave radiation is diurnally varied based on the formulas of Danabagoslu et al. (2006). In addition, the input of short-wave radiation lessens by 10% when the precipitation data is significant.

3. Results

3-1 Comparison of simulated temperature with observations

Figure 1 shows time series of observed and simulated temperature at the location of moored buoy. Even though simulated temperature at the 100 m depth was poorly reproduced in MRI.COM, the model well reproduced the evolution of observed temperature at the 0 m depth. After the passage of Tina, near-inertial oscillation was salient at the 50 m depth, which was not reproduced in MRI.COM. On the other hand, MRI.COM could reproduce the deepening of mixed-layer after the passage of Winnie.

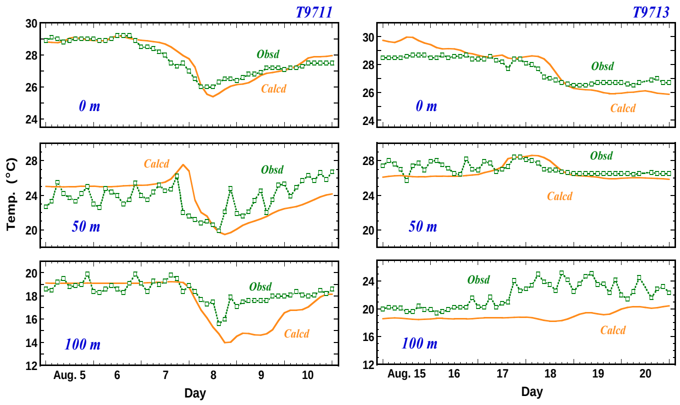

Figure 1 Time series of observed (green lines) and simulated (orange lines) temperature at 0 m (upper panels), 50 m (middle panels) and 100 m (lower panels) depths. Left panels showed the results in Typhoon Tina and right ones in Typhoon Winnie.

The results of the difference in two time series suggest that dynamics and thermodynamics related to the variations of temperature are considered to be different between Tina and Winnie.

3.2 Typhoon Tina

Figure 2 shows time series of simulated sea temperature at the location of moored buoy. First, a mixed layer deepens around 7 August. Subsequently, salient upwelling occurs from 7 to 9 August. Seasonal thermocline is raised to the surface during the passage of Tina. Figure 3 shows the latitude-depth section of simulated temperature and horizontal currents across 126.25˚E at 1500 UTC 7 August. At that time, the moored buoy is underneath the center of Tina. Cold water below the seasonal thermocline is transported to the mixed layer due to strong upwelling over the continental shelf. Behind Tina (the ocean response to Tina after its passage), near-inertial oscillation is induced at the mixed-layer base.

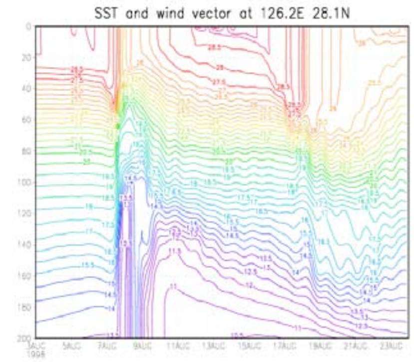

Figure 2 Time series of sea temperature at the moored buoy (28.1˚N,126.2˚E) from 3 to 19 August.

3.3 Typhoon Winnie

On the other hand, no salient upwelling occurs during the passage of Winnie. Figure 4 shows the latitude-depth section of simulated temperature and horizontal currents across 126.25 ˚E at 0600 UTC 18 August. Around the location of moored buoy, a mixed layer is relatively deep compared with that shown in Figure 3. In fact, Winnie passes 25.4 ˚N, 126.25˚E south (the moored buoy during the period from 1800 UTC to 2100 UTC 17 August. Because the size of Winnie defined as the radius of 15 m s^{-1} wind speed) is relatively large, long-lasting vertical turbulent mixing induced by strong wind continuously deepens the mixed layer and lowers the mixed-layer temperature.

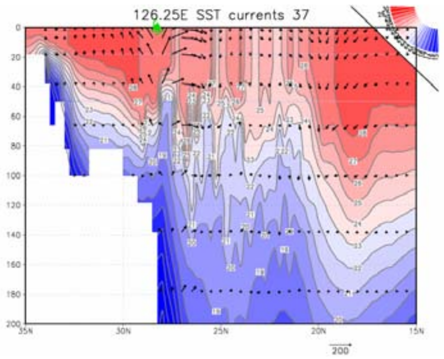

Figure 3 Latitude-depth section of simulated temperature and horizontal currents across 126.25˚E at the 37 steps every 3 hours, corresponding to 1500 UTC 7 August.

Although the oceanic dynamics and thermodynamic at the location of moored buoy are different between Tina and Winnie, these typhoons have a significant impact on the sudden variations of oceanic $p$$CO_2$. We need to clarify the process of acceleration in the uptake transport of oceanic CO_2 caused by typhoons and the impact of typhoon-induced increase in CO_2 fluxes on the climate.

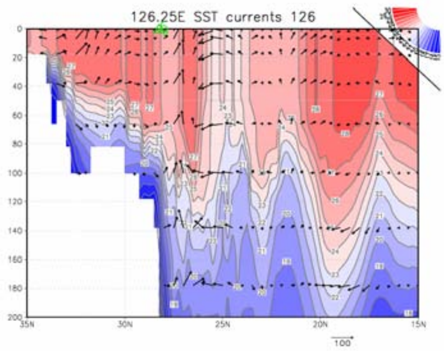

Figure 4 Same as Figure 2 except at the 126 steps every 3 hours, corresponding to 0600 UTC 18 August.

References

Danabasoglu, G., W.G. Large, J.J. Tribbia, P.R. Gent, B.P. Briegleb, and J.C. McWilliams, 2006: Diurnal Coupling in the Tropical Oceans of CCSM3. J. Climate, 19, 2347–2365.

Ishikawa, I., H. Tsujino, M. Hirabara, H. Nakano, T. Yasuda and H. Ishizaki, 2005: Meteorological Research Institute Community Ocean Model (MRI.COM) Manual. Technical Reports of the Meteorological Research Institute, 47, (in Japanese).

Nemoto, K., T. Midorikawa, A. Wada, K. Ogawa, S. Takatani, H. Kimoto, M. Ishii, H.Y. Inoue, 2009: Continuous observations of atmospheric and oceanic CO2 using a moored buoy in the East China Sea: Variations during the passage of typhoons, Deep Sea Research Part II: Topical Studies in Oceanography, In Press.

Wada, A., H. Niino and H. Nakano, 2009: Roles of Vertical Turbulent Mixing in the Ocean Response to Typhoon Rex (1998), J. Oceanogr. Accepted.

The impact of pre-existing oceanic condition on the ocean response to Typhoon Hai-Tang in 2005

Akiyoshi Wada [1*], Norihisa Usui[1], Kanako Sato[2] and Yoshimi Kawai[2]

1) Meteorological Research Institute, Tsukuba, Ibaraki, 305-0052, JAPAN

2) Japan Agency for Marine-Earth Science and Technology, 2-15 Natsushima-Cho, Yokosuka, 237-0061, JAPAN.

*awada@mri-jma.go.jp

1. Introduction

Sea surface cooling (SSC) by the passage of tropical cyclones is known to be mainly caused by the Ekman pumping and vertical turbulent mixing. The impact of pre-existing oceanic condition (for examples, mixed-layer depth and temperature gradient in the thermocline) on SSC is thought to be relatively small compared with the Ekman pumping and vertical turbulent mixing. Recently, Zheng et al. (2008) suggested the importance of pre-existing oceanic condition on SSC caused by the passage of Typhoon Hai-Tang in 2005. They concluded that SSC caused by the Ekman pumping was not significant due to fast translation of Hai-Tang (5-8 m s^{-1}). Although the impact of pre-existing oceanic condition on SSC underlying Hai-Tang is significant, SSC caused by the passage of Hai-Tang may be influenced by the Ekman pumping to some extent because cyclonic wind stress results in the divergent flow at the sea surface which enables the water beneath the typhoon to transport outside and to raise the seasonal thermocline. In order to confirm the above-mentioned typhoon-induced dynamics during the passage of Hai-Tang, we investigated the impact of pre-existing oceanic condition on the ocean response to Hai-Tang using the Meteorological Research Institute Community Ocean Model (MRI.COM).

2. Experiment Design

First, we perform a numerical simulation using the North Pacific version of MRI.COM. The integration time is 2 months with nudging daily data of sea temperature and salinity on 11 August 2005, obtained from the oceanic reanalysis data. Second, we perform a numerical simulation by the same version except that the integration time is 11 days and the run is performed without nudging daily data of sea temperature and salinity on 11 August 2005. The purpose of the second run is to make initial and lateral boundary conditions for the third run. Third, we perform a numerical simulation using the regional version of MRI.COM. The integration time is 11 days. The computational domain for the regional model is 120-160°E, 10-50°N. The horizontal resolution is 0.25° and the number of vertical levels is 54. The time step is 10 minutes. The mixed-layer scheme of Noh and Kim (1999) is used in the present study. These three procedures are the same as those of Wada et al., (2009).

NCEP R2 atmospheric reanalysis dataset with a grid spacing of 1.875° is used for making atmospheric forcings such as short-wave and long-wave radiation, sensible and latent heat fluxes, water flux and wind stress. In addition, the Rankine vortex created by using the RSMC best track data is used for the third run (see Wada et al., 2009). Short-eave radiation is diurnally varied based on the formulas of Danabagoslu et al. (2006). The input of short-wave radiation lessens by 10% when the precipitation data is significant. Not only NCEP R2 data but also hourly GsMAP data (http://www.radar.aero.osakafu-u.ac.jp/~gsmap/pdf/gsmap_mwr_j_web.pdf) are used for estimating hourly precipitation data. When there is no precipitation data, the precipitation is expressed as a function of wind speed (Jacob and Koblinsky, 2007): P (mm $hour^{-1}$) =0.0016 x (v – 25) where P indicates precipitation and v wind speed.

3. Results

Figure 1 shows horizontal distributions of simulated sea surface temperature (SST: °C) and sea surface height (SSH: cm) at 120h. Around 21-22°N, 126°E where Hai-Tang passed, SSH was low in 2005 (Fig.1a), while that was relatively high in 1999 (Fig. 1b). The difference in SSH between 1999 and 2005 was independent of the ocean response to Hai-Tang because Hai-Tang was positioned around 20°N, 130°E at 120h. Figure 2 shows latitude-depth sections of sea temperature from the surface to 100 m depth at 120h. In 2005, the seasonal thermocline is shallow around 21-22°N (Fig. 2a), while the seasonal thermocline is relatively deep in 1999 (Fig. 2b). Figure 3 shows the latitude-depth sections of sea temperature at

196h. Salient upwelling occurs at 21° and 22°N in 2005, resulting in salient SSC after the passage of Hai-Tang (Fig. 3a). However, SSC is not salient in 1999 (Fig. 3b). Therefore, pre-existing oceanic condition affects the formation of SSC caused by the typhoon-induced upwelling (mainly caused by the Ekman pumping).

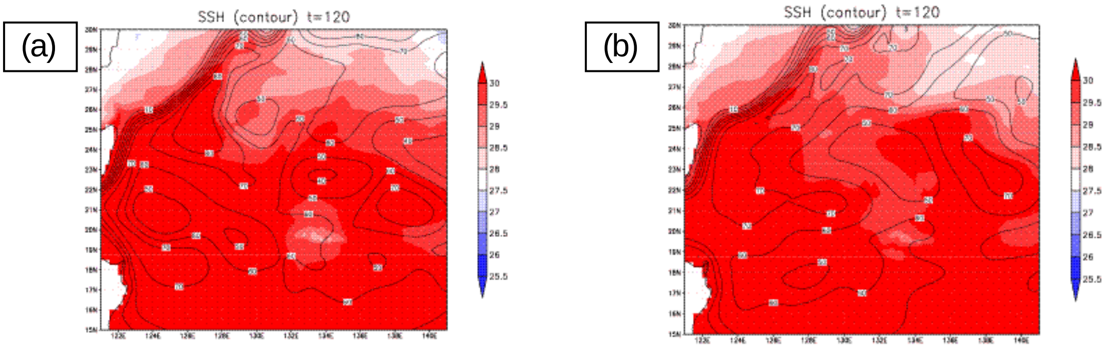

Figure 1 Simulated sea surface temperature and sea surface height at 120h (a) in the 2005 and (b) in the 1999 fields.

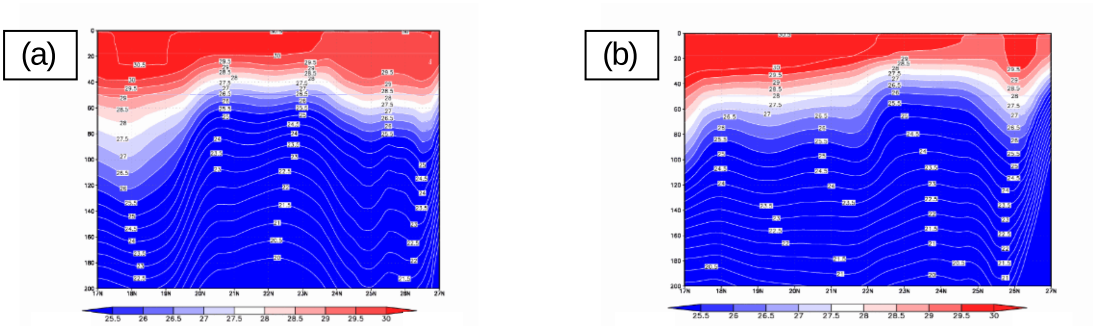

Figure 2 Latitude-depth section of simulated sea temperature across 126°E at 120h (a) in the 2005 and (b) in the 1999 fields.

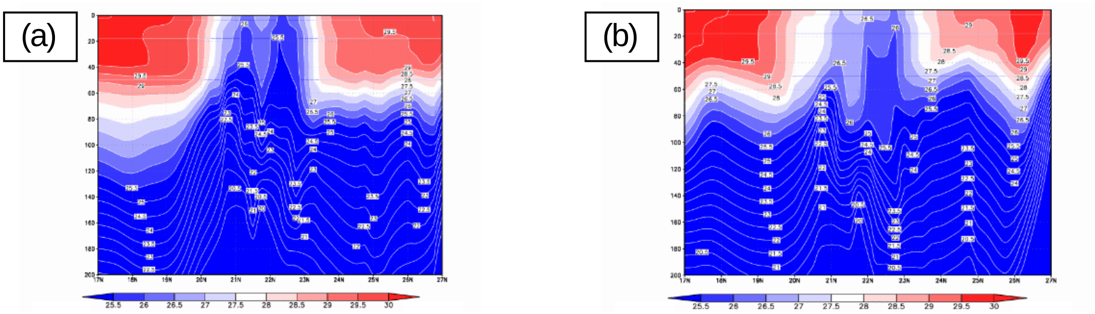

Figure 3 Same as Figure 2 except at 196h.

References

Danabasoglu, G., W.G. Large, J.J. Tribbia, P.R. Gent, B.P. Briegleb, and J.C. McWilliams, 2006: Diurnal Coupling in the Tropical Oceans of CCSM3. J. Climate, 19, 2347–2365.

Ishikawa, I., H. Tsujino, M. Hirabara, H. Nakano, T. Yasuda and H. Ishizaki, 2005: Meteorological Research Institute Community Ocean Model (MRI.COM) Manual. Technical Reports of the Meteorological Research Institute, 47, (in Japanese).

Noh, Y., and H. Jin Kim, 1999: Simulations of temperature and turbulence structure of the oceanic boundary layer with the improved near-surface process, J. Geophys. Res., 104(C7), 15,621–15,634.

Jacob, S.D., and C.J. Koblinsky, 2007: Effects of Precipitation on the Upper-Ocean Response to a Hurricane. Mon. Wea. Rev., 135, 2207–2225.

Wada, A., H. Niino and H. Nakano, 2009: Roles of Vertical Turbulent Mixing in the Ocean Response to Typhoon Rex (1998), J. Oceanogr. Accepted.

Zheng, Z.-W., C.-R. Ho, and N.-J. Kuo, 2008: Importance of pre-existing oceanic conditions to upper ocean response induced by Super Typhoon Hai-Tang, Geophys. Res. Lett., 35, L20603, doi:10.1029/2008GL035524.